Hindawi
Shock and Vibration
Volume 2017, Article ID 2617534, 11 pages
https://doi.org/10.1155/2017/2617534

Research Article

Scaling Mode Shapes in Output-Only Structure by a Mass-Change-Based Method

Liangliang Yu and Hanwen Song

School of Aerospace Engineering and Applied Mechanics, Tongji University, Shanghai 200092, China

Correspondence should be addressed to Hanwen Song; hwsong@tongji.edu.cn

Received 5 February 2017; Accepted 27 March 2017; Published 26 April 2017

Academic Editor: Tai Thai

Copyright © 2017 Liangliang Yu and Hanwen Song. This is an open access article distributed under the Creative Commons Attribution License, which permits unrestricted use, distribution, and reproduction in any medium, provided the original work is properly cited.

A mass-change-based method based on output-only data for the rescaling of mode shapes in operational modal analysis (OMA) is introduced. The mass distribution matrix, which is defined as a diagonal matrix whose diagonal elements represent the ratios among the diagonal elements of the mass matrix, is calculated using the unscaled mode shapes. Based on the theory of null space, the mass distribution vector or mass distribution matrix is obtained. A small mass with calibrated weight is added to a certain location of the structure, and then the mass distribution vector of the modified structure is estimated. The mass matrix is identified according to the difference of the mass distribution vectors between the original and modified structures. Additionally, the universal set of modes is unnecessary when calculating the mass distribution matrix, indicating that modal truncation is allowed in the proposed method. The mass-scaled mode shapes estimated in OMA according to the proposed method are compared with those obtained by experimental modal analysis. A simulation is employed to validate the feasibility of the method. Finally, the method is tested on output-only data from an experiment on a five-storey structure, and the results confirm the effectiveness of the method.

1. Introduction

Operational modal analysis (OMA) is an engineering field in which the modal properties of structures under ambient vibrations are studied [1]. Its development can be traced to 1965, when the method using the cross-correlation function to estimate the frequency response function (FRF) was proposed by Clarkson and Mercer [2], which was also the origin of using the cross-correlation function instead of the impulse response function (IRF) to identify the mode parameters in cases where the excitation is unknown. After approximately 50 years of development, especially due to studies of autoregressive moving average (ARMA) [3], random decrement technique (RDT) [4], operational deflection shapes (ODS) [5], natural excitation technique (NExT) [6], and stochastic subspace identification (SSI) [7], OMA has matured and has been extended to a wider range of applications in engineering.

Furthermore, if the identified mode parameters are further used to predict structural response, structural modification, or health monitoring, the FRF or IRF should be identified. In fact, the FRF is obtained using experimental modal analysis (EMA) in the laboratory. Since the boundary conditions of the structure during a laboratory test are not entirely identical with real in-operation working conditions of the structure, the FRF of the system in the laboratory is different from that in an operating state. Therefore, reconstructing the FRF based on the mode parameters (natural frequencies, damping ratios, and mass-scaled mode shapes) identified using the OMA method is necessary. Because the excitation cannot be measured in OMA, the mode shapes cannot be normalized or scaled by mass. As a consequence, an additional procedure to obtain the mass-scaled modal shapes is needed. In the past few years, many methods have been proposed to solve this problem. Doebling and Farrar [8] used a finite-element model (FEM) mass matrix that is reduced to the measurement degree of freedom (DOF) to normalize the mode shapes, according to the work of Guyan [9]. However, their method is only valid for the lower-frequency modes. Another method used the mode parameters identified using the OMA technology to upgrade the FEM, from which the mass matrix that scales the mode shapes was obtained [10–15]. Randall et al. [16] strictly limited

the form of excitation and developed cepstral methods for updating mode parameters identified using the OMA method when the logarithmic spectrum of the excitation is smooth and flat enough. Using the mass perturbation as a mode shape scaling method originated from Parloo et al. [17, 18]. By adding one or more masses whose weights are calibrated to the structure, the operational mode shapes can be mass-scaled by the shift in mode frequencies between the original and modified structures. On the basis of this idea, much work has been done. The approximate formula for determination of the scaling factors based on the frequency shift when introducing mass perturbation on the structure was derived directly from the governing equation of motion [19]. It explained how testing should be performed in order to significantly reduce approximation errors. The uncertainties of the estimated scaling factors were also investigated [20]. An exact formulation computing the square of the scaling factors was given by Bernal [21, 22]. This formulation can be used in structures with both non-closely spaced modes and closely spaced modes. López-Aenlle et al. [23] provided two new exact formulations for scaling factors, illustrated the large difference in accuracy between the approximate and exact formulations, and confirmed that the results are similar only when the mass perturbation is relatively small. Taking into account a drawback that the first mode of a structure is less sensitive to the mass perturbation, a new mass-stiffness perturbation method was suggested to scale the mode shapes [24]. A procedure to optimize the mass perturbation strategy was proposed by López-Aenlle et al. [25, 26], which used the mode parameters (natural frequencies and shapes) of the original structure as basic information. Different mass perturbation methods were applied to estimate the scaling factors of a 15-T concrete slab by Fernández et al. [27]. The results showed that all of the methods estimate the scaling factors with good accuracy when an appropriate mass change strategy is adopted. Poozesh et al. employed the drive point scaling method to scale optically measured operating deflection shapes (ODS) [28]. Additionally, they demonstrated the benefits and drawbacks of the mass sensitivity technique. However, the accuracy of the mass matrix obtained by the finite-element method commonly depends on the accuracy of the modeling of the structure. Meanwhile, the mass change in the aforementioned method should not be too high in order to minimize the difference of the mode shapes between the original and modified structures.

In this paper, the mass distribution matrix is defined and calculated using unscaled mode shapes given that the structure is discrete and the mass matrix is diagonal [8, 9, 29]. The mass matrix is the product of the mass distribution matrix and a coefficient. Then, a small mass with calibrated weight is added to a certain location of the structure, and the mass distribution vector of the structure is estimated. It is noteworthy that removing a small mass with calibrated weight from a certain location of the structure is also feasible. Based on the difference of the mass distribution vectors between the original and modified structures, the mass matrix is identified. Mode shapes are scaled by the mass matrix. It is also worth noting that a universal set of modes is unnecessary when calculating the mass distribution matrix. This means that modal truncation is allowed in the proposed method.

The rest of this paper is organized as follows. In Section 2, the mass distribution matrix of the structure is defined and calculated. The mass matrix is obtained based on the method that a small mass with calibrated weight is added to a certain DOF of the structure. Then, the unscaled mode shapes are scaled by the mass matrix. Finally, a simulation and an experiment are presented in Sections 3 and 4, respectively.

2. Scaling Mode Shapes

In this section, the mass distribution matrix is defined and calculated by unscaled mode shapes. Then, the mass matrix is obtained by the mass change method and the mode shapes are scaled by the mass matrix. Finally, modal truncation is discussed.

2.1. Mass Distribution Matrix. The equation of motion of a linear time-invariant discrete system with N DOFs can be written as

$$[M]\{\ddot{x}(t)\} + [C]\{\dot{x}(t)\} + [K]\{x(t)\} = \{f(t)\}, \quad (1)$$

where $[M]$, $[C]$, and $[K]$ represent the mass, damping, and stiffness matrices, respectively. $[M]$ is a real, symmetric, positive definite matrix. $[C]$ and $[K]$ are real, symmetric, and positive or semipositive definite matrices. t denotes time. $\{f(t)\}$ is the excitation, and $\{x(t)\}$ represents the displacement response vector.

According to the property that mode shapes are weighted orthogonal with respect to the mass matrix, one has

$$[\Psi]^T [M][\Psi] = [I], \quad (2)$$

where $[\Psi]$ is the mass-scaled mode shape matrix and $[I]$ is the identity matrix.

The relation between the unscaled or arbitrary scaled mode shape matrix and the mass-scaled mode shape matrix can be expressed as

$$[\Phi] = [\Psi][\alpha] = \left[\alpha_1 \begin{Bmatrix} \psi_{11} \\ \psi_{21} \\ \vdots \\ \psi_{N1} \end{Bmatrix} \alpha_2 \begin{Bmatrix} \psi_{12} \\ \psi_{22} \\ \vdots \\ \psi_{N2} \end{Bmatrix} \cdots \alpha_N \begin{Bmatrix} \psi_{1N} \\ \psi_{2N} \\ \vdots \\ \psi_{NN} \end{Bmatrix} \right], \quad (3)$$

where $[\Phi]$ is the unscaled or arbitrarily scaled mode shape matrix. The scaling factor $[\alpha]$ is a diagonal matrix with unknown but positive elements.

Substituting (3) into (2) yields

$$[\Phi]^T [M][\Phi] = [\alpha]^2. \quad (4)$$

On the basis of the assumption that the structure is a discrete system whose mass matrix can be assumed to be

diagonal [8, 9, 29], the expanded form of (4) can be written as

$$\begin{bmatrix} \phi_{11} & \phi_{12} & \cdots & \phi_{1i} & \cdots & \phi_{1N} \\ \phi_{21} & \phi_{22} & \cdots & \phi_{2i} & \cdots & \phi_{2N} \\ \vdots & \vdots & \cdots & \vdots & \cdots & \vdots \\ \phi_{N1} & \phi_{N2} & \cdots & \phi_{Ni} & \cdots & \phi_{NN} \end{bmatrix}^T \operatorname{diag}(\{m\}) \cdot \begin{bmatrix} \phi_{11} & \phi_{12} & \cdots & \phi_{1j} & \cdots & \phi_{1N} \\ \phi_{21} & \phi_{22} & \cdots & \phi_{2j} & \cdots & \phi_{2N} \\ \vdots & \vdots & \cdots & \vdots & \cdots & \vdots \\ \phi_{N1} & \phi_{N2} & \cdots & \phi_{Nj} & \cdots & \phi_{NN} \end{bmatrix} = \operatorname{diag}\left(\begin{Bmatrix} \alpha_1^2 \\ \alpha_2^2 \\ \vdots \\ \alpha_N^2 \end{Bmatrix} \right), \tag{5}$$

where

$$\{m\} = \{m_1 \;\; m_2 \;\; \cdots \;\; m_N\}^T, \tag{6}$$

and diag($\{m\}$) returns a square diagonal matrix with the elements of vector $\{m\}$ on the main diagonal.

Considering the symmetry on the left-hand side of (5), $N(N+1)/2$ equations can be obtained from (5), in which m_i $(i = 1, 2, \ldots, N)$ is the independent variable.

When $i = j$, N equations can be extracted from (5) as

$$\begin{bmatrix} \phi_{11}\phi_{11} & \phi_{21}\phi_{21} & \cdots & \phi_{N1}\phi_{N1} \\ \phi_{12}\phi_{12} & \phi_{22}\phi_{22} & \cdots & \phi_{N2}\phi_{N2} \\ \vdots & \vdots & \ddots & \vdots \\ \phi_{1N}\phi_{1N} & \phi_{2N}\phi_{2N} & \cdots & \phi_{NN}\phi_{NN} \end{bmatrix} \begin{Bmatrix} m_1 \\ m_2 \\ \vdots \\ m_N \end{Bmatrix} = \begin{Bmatrix} \alpha_1^2 \\ \alpha_2^2 \\ \vdots \\ \alpha_N^2 \end{Bmatrix}. \tag{7}$$

Equation (7) cannot be solved since the scaling factor matrix $[\alpha]$ is unknown.

When $i < j$, $N(N-1)/2$ equations can be extracted from (5) as

$$[A]\{m\} = \{0\}, \tag{8}$$

where

$$[A] = \begin{bmatrix} \phi_{11}\phi_{12} & \phi_{21}\phi_{22} & \cdots & \phi_{N1}\phi_{N2} \\ \phi_{11}\phi_{13} & \phi_{21}\phi_{23} & \cdots & \phi_{N1}\phi_{N3} \\ \vdots & \vdots & \ddots & \vdots \\ \phi_{11}\phi_{1N} & \phi_{21}\phi_{2N} & \cdots & \phi_{N1}\phi_{NN} \\ \hline \phi_{12}\phi_{13} & \phi_{22}\phi_{23} & \cdots & \phi_{N2}\phi_{N3} \\ \phi_{12}\phi_{14} & \phi_{22}\phi_{24} & \cdots & \phi_{N2}\phi_{N4} \\ \vdots & \vdots & \ddots & \vdots \\ \phi_{12}\phi_{1N} & \phi_{22}\phi_{2N} & \cdots & \phi_{N2}\phi_{NN} \\ \hline \vdots & \vdots & \vdots & \vdots \\ \phi_{1,N-1}\phi_{1N} & \phi_{2,N-1}\phi_{2N} & \cdots & \phi_{N,N-1}\phi_{NN} \end{bmatrix}_{N(N-1)/2 \times N}. \tag{9}$$

Owing to the symmetry on the left-hand side of (5), the case when $i > j$ is similar to that when $i < j$ and is omitted here. In (8), there are $N(N-1)/2$ equations. $\{m\}$ is the null space of $[A]$. Given that $\{m\}$ exists and is unique, the dimension of the null space of $[A]$ is 1. Therefore, the rank of $[A]$ is $N-1$. The mass distribution vector $\{\widetilde{M}\}$, which denotes the ratios among the elements of $\{m\}$, is the unique basis of the null space of $[A]$. Since singular value decomposition (SVD) is an efficient method of calculating the null space of a matrix, it is adopted to obtain $\{\widetilde{M}\}$:

$$[A] = [U][S][V]^T. \tag{10}$$

Because the rank of $[A]$ is $N-1$ and the singular values in $[S]$ are sorted in descending order, $\{\widetilde{M}\}$ can be obtained as

$$\left\{\widetilde{M}\right\} = \{V\}_N, \tag{11}$$

where $\{\widetilde{M}\}$ is scaled by its 2-norm because $[V]$ is a unit orthogonal matrix. Consequently, the mass distribution matrix is expressed as

$$\left[\widetilde{M}\right] = \operatorname{diag}\left(\left\{\widetilde{M}\right\}\right). \tag{12}$$

2.2. Mass Matrix. A small mass with calibrated weight Δm_k is added to the DOF k of the structure. According to the method similar to that used in Section 2.1, the mass distribution vector of the structure modified by Δm_k, denoted as $\{\widetilde{M}^\delta\}$, can be obtained.

Owing to the fact that $\{\widetilde{M}\}$ is scaled by its 2-norm, $\{\widetilde{M}\}$ can be rewritten as

$$\left\{\widetilde{M}\right\} = \left\{ \frac{m_1}{\|\{m\}\|} \;\; \cdots \;\; \frac{m_k}{\|\{m\}\|} \;\; \cdots \;\; \frac{m_N}{\|\{m\}\|} \right\}^T, \tag{13}$$

where $\|\{m\}\|$ is the 2-norm of vector $\{m\}$.

Similarly, $\{\widetilde{M}^{\delta}\}$ can be rewritten as

$$\left\{\widetilde{M}^{\delta}\right\} = \left\{ \frac{m_1}{\left(\Delta m_k^2 + 2m_k\Delta m_k + \|\{m\}\|^2\right)^{1/2}} \cdots \frac{m_k + \Delta m_k}{\left(\Delta m_k^2 + 2m_k\Delta m_k + \|\{m\}\|^2\right)^{1/2}} \cdots \frac{m_N}{\left(\Delta m_k^2 + 2m_k\Delta m_k + \|\{m\}\|^2\right)^{1/2}} \right\}^T. \quad (14)$$

Combining the kth equation in (13) and the kth equation in (14), the following equations can be obtained:

$$\frac{m_k}{\|\{m\}\|} = \widetilde{M}_k,$$

$$\frac{m_k + \Delta m_k}{\left(\Delta m_k^2 + 2m_k\Delta m_k + \|\{m\}\|^2\right)^{1/2}} = \widetilde{M}_k^{\delta}. \quad (15)$$

Solving the equations in (15), one obtains

$$\|\{m\}\| = \frac{\widetilde{M}_k\left(1 - \left(\widetilde{M}_k^{\delta}\right)^2\right) + \sqrt{\widetilde{M}_k^2\left(\widetilde{M}_k^{\delta}\right)^4 - \widetilde{M}_k^2\left(\widetilde{M}_k^{\delta}\right)^2 - \left(\widetilde{M}_k^{\delta}\right)^4 + \left(\widetilde{M}_k^{\delta}\right)^2}}{\left(\left(\widetilde{M}_k^{\delta}\right)^2 - \widetilde{M}_k^2\right)}\Delta m_k. \quad (16)$$

Substituting (16) into (6) and (13) yields

$$\{m\} = \frac{\widetilde{M}_k\left(1 - \left(\widetilde{M}_k^{\delta}\right)^2\right) + \sqrt{\widetilde{M}_k^2\left(\widetilde{M}_k^{\delta}\right)^4 - \widetilde{M}_k^2\left(\widetilde{M}_k^{\delta}\right)^2 - \left(\widetilde{M}_k^{\delta}\right)^4 + \left(\widetilde{M}_k^{\delta}\right)^2}}{\left(\left(\widetilde{M}_k^{\delta}\right)^2 - \widetilde{M}_k^2\right)}\Delta m_k \left\{\widetilde{M}\right\}. \quad (17)$$

Then, the mass matrix of the structure is obtained as

$$[M] = \operatorname{diag}(\{m\}) = \frac{\widetilde{M}_k\left(1 - \left(\widetilde{M}_k^{\delta}\right)^2\right) + \sqrt{\widetilde{M}_k^2\left(\widetilde{M}_k^{\delta}\right)^4 - \widetilde{M}_k^2\left(\widetilde{M}_k^{\delta}\right)^2 - \left(\widetilde{M}_k^{\delta}\right)^4 + \left(\widetilde{M}_k^{\delta}\right)^2}}{\left(\left(\widetilde{M}_k^{\delta}\right)^2 - \widetilde{M}_k^2\right)}\Delta m_k \cdot \left[\widehat{M}\right]. \quad (18)$$

2.3. Scaling Factor. Since the mass matrix has been obtained in Section 2.2, the mode shape matrix can be scaled. Substituting (18) into (4), one has

$$[\alpha]^2 = \frac{\widetilde{M}_k\left(1 - \left(\widetilde{M}_k^{\delta}\right)^2\right) + \sqrt{\widetilde{M}_k^2\left(\widetilde{M}_k^{\delta}\right)^4 - \widetilde{M}_k^2\left(\widetilde{M}_k^{\delta}\right)^2 - \left(\widetilde{M}_k^{\delta}\right)^4 + \left(\widetilde{M}_k^{\delta}\right)^2}}{\left(\left(\widetilde{M}_k^{\delta}\right)^2 - \widetilde{M}_k^2\right)}\Delta m_k [\Phi]^T \left[\widehat{M}\right][\Phi]. \quad (19)$$

Since the matrix $[\Phi]^T[\widehat{M}][\Phi]$ is diagonal and all diagonal elements are positive, $[\alpha]$ can thus be written as

$$[\alpha] = \left(\frac{\widetilde{M}_k\left(1 - \left(\widetilde{M}_k^{\delta}\right)^2\right) + \sqrt{\widetilde{M}_k^2\left(\widetilde{M}_k^{\delta}\right)^4 - \widetilde{M}_k^2\left(\widetilde{M}_k^{\delta}\right)^2 - \left(\widetilde{M}_k^{\delta}\right)^4 + \left(\widetilde{M}_k^{\delta}\right)^2}}{\left(\left(\widetilde{M}_k^{\delta}\right)^2 - \widetilde{M}_k^2\right)}\Delta m_k \right)^{1/2} \cdot \sqrt{[\Phi]^T \left[\widehat{M}\right][\Phi]}, \quad (20)$$

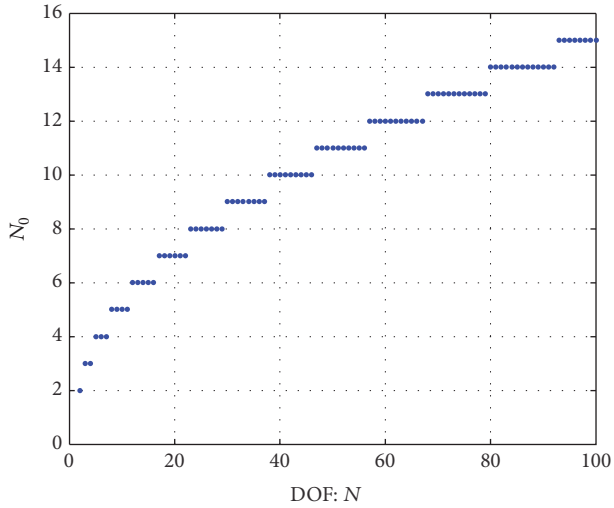

Figure 1: Relationship between N and N_0.

where $\sqrt{[\Phi]^T[\widehat{M}][\Phi]}$ represents the square root of the diagonal element of matrix $[\Phi]^T[\widehat{M}][\Phi]$.

Substituting (20) into (3), one can scale the mode shapes by the mass matrix:

$$[\Psi] = \left(\frac{\widetilde{M}_k \left(1 - \left(\widetilde{M}_k^{\delta}\right)^2\right) + \sqrt{\widetilde{M}_k^2 \left(\widetilde{M}_k^{\delta}\right)^4 - \widetilde{M}_k^2 \left(\widetilde{M}_k^{\delta}\right)^2 - \left(\widetilde{M}_k^{\delta}\right)^4 + \left(\widetilde{M}_k^{\delta}\right)^2}}{\left(\left(\widetilde{M}_k^{\delta}\right)^2 - \widetilde{M}_k^2\right)} \Delta m_k \right)^{-1/2} [\Phi] \cdot \left(\sqrt{[\Phi]^T \left[\widehat{M}\right] [\Phi]} \right)^{-1}. \quad (21)$$

2.4. Modal Truncation. Generally, a universal set of modes cannot be obtained due to modal truncation. When the order of the modes is truncated as T ($T \le N$), (8) becomes

$$\left[\widetilde{A}\right]_{T(T-1)/2\times N} \{m\}_N = \{0\}_N. \quad (22)$$

Considering the fact that the rank of $[\widetilde{A}]$ is $N-1$, both T and N should satisfy the following inequality:

$$\frac{1}{2} T (T-1) \ge N - 1. \quad (23)$$

Solving the inequality in (23), one has

$$T \ge \text{ceil}\left(\frac{\sqrt{8N-7}+1}{2} \right) = N_0, \quad (24)$$

where ceil$((\sqrt{8N-7}+1)/2)$ means rounding $(\sqrt{8N-7}+1)/2$ to the nearest integer greater than or equal to $(\sqrt{8N-7}+1)/2$ and N_0 is the smallest positive integer that satisfies the inequality in (24). The details of the relationship between N and N_0 are presented in Figure 1.

When $N \ge 4$, as is shown in Figure 1, $N_0 < N$. This means that the universal set of modes is unnecessary when calculating the mass distribution matrix. In other words, the modal truncation is allowed. The growth rate of N_0 is much smaller than the growth rate of N. When N is sufficiently large, it follows that $N_0 \ll N$.

It is worth noting that (24) is the premise of calculating the mass distribution matrix in this paper. If the total number of natural modes identified is smaller than N_0, the mass matrix or mass distribution matrix cannot be obtained by the aforementioned method.

Considering the modal truncation, when arbitrary N_0 mode shapes are taken from all T mode shapes, (22) can be written as

$$\left[{}^i\widetilde{A}\right]_{N_0(N_0-1)/2\times N} \{m\}_i = \{0\}, \quad (25)$$

where $i = 1, 2, \ldots, C_T^{N_0}$ ($C_T^{N_0}$ is the total number of combinations of taking N_0 items at a time from T). According to (11), $C_T^{N_0}$ mass distribution vectors can be obtained.

Similarly, when arbitrary $N_0 + 1$ mode shapes are taken from all T ones, (22) can be written as

$$\left[{}^i\widetilde{A}\right]_{N_0(N_0+1)/2\times N} \{m\}_i = \{0\}, \quad (26)$$

where $i = C_T^{N_0}+1, C_T^{N_0}+2, \ldots, C_T^{N_0}+C_T^{N_0+1}$. Thus, $C_T^{N_0+1}$ mass distribution vectors can be extracted.

Inductively, when T mode shapes are taken, C_T^T mass distribution vector can be obtained.

Using the enumerating method, S_T mass distribution vectors can be obtained from T identified modes; namely,

$$S_T = C_T^{N_0} + C_T^{N_0+1} + C_T^{N_0+2} + \cdots + C_T^T. \tag{27}$$

Theoretically, the mass distribution vectors calculated by different mode shape combinations should be identical.

3. Simulation

In this section, a 10-DOF structure is designed to verify the method of scaling mode shapes.

The mass matrix is

$$\begin{aligned}&\left[M_{\text{given}}\right]\\ &= \text{diag}\left(\left\{3.8 \;\; 13.0 \;\; 4.6 \;\; 3.8 \;\; 0.6 \;\; 1.8 \;\; 0.6 \;\; 18.8 \;\; 3.2 \;\; 2.0\right\}^T\right) \text{ kg.}\end{aligned} \tag{28}$$

The stiffness matrix is

$$\left[K_{\text{given}}\right] = \begin{bmatrix} 317800 & -88000 & -16300 & -63100 & -70700 & 0 & 0 & 0 & 0 & 0 \\ -88000 & 312600 & -19700 & -16800 & -4600 & -96900 & 0 & 0 & 0 & 0 \\ -16300 & -19700 & 279600 & -32800 & -65200 & -35200 & -65200 & 0 & 0 & 0 \\ -63100 & -16800 & -32800 & 280200 & -33000 & -65800 & -30400 & -25600 & 0 & 0 \\ -70700 & -4600 & -65200 & -33000 & 342000 & -73500 & -19100 & -29800 & -46100 & 0 \\ 0 & -96900 & -35200 & -65800 & -73500 & 368100 & -67100 & -20200 & -3000 & -6400 \\ 0 & 0 & -65200 & -30400 & -19100 & -67100 & 311500 & -44000 & -41100 & -44600 \\ 0 & 0 & 0 & -25600 & -29800 & -20200 & -44000 & 163500 & -5400 & -38500 \\ 0 & 0 & 0 & 0 & -46100 & -3000 & -41100 & -5400 & 192800 & -97200 \\ 0 & 0 & 0 & 0 & 0 & -6400 & -44600 & -38500 & -97200 & 186700 \end{bmatrix} \text{ N/m.} \tag{29}$$

Consequently, the natural mode frequencies are 8.34, 18.92, 26.67, 33.74, 42.02, 48.69, 54.57, 70.05, 116.68, and 122.89 Hz. Taking the damping ratio for every order of the structure to be $\zeta_1 = 0.008$, $\zeta_2 = 0.008$, $\zeta_3 = 0.008$, $\zeta_4 = 0.007$, $\zeta_5 = 0.007$, $\zeta_6 = 0.007$, $\zeta_7 = 0.006$, $\zeta_8 = 0.006$, $\zeta_9 = 0.006$, and $\zeta_{10} = 0.006$, the damping matrix of the system is computed by

$$\left[C_{\text{given}}\right] = [\Phi]^{-T} \,\text{diag}\left\{\widetilde{c}_1 \;\cdots\; \widetilde{c}_r \;\cdots\; \widetilde{c}_N\right\} [\Phi]^{-1}, \tag{30}$$

where $\widetilde{c}_r = 2\zeta_r \widetilde{m}_r \omega_r$, $\widetilde{m}_r = \{\Phi\}_r^T [M_{\text{given}}] \{\Phi\}$, and $r = 1, 2, \ldots, 10$.

3.1. Mass Distribution Matrix. The loads on the structure are uncorrelated random signals subjected to Gaussian distribution. In this simulation, they fit $N(0, 10000)$, $N(0, 10000)$, $N(0, 10000)$, $N(0, 8100)$, $N(0, 8100)$, $N(0, 8100)$, $N(0, 6400)$, $N(0, 6400)$, $N(0, 6400)$, and $N(0, 6400)$, where $N(\mu, \sigma^2)$ denotes a Gaussian distribution with μ being a mean value and σ^2 the variance. In order to illustrate the advantage of modal truncation, all of the random signals are filtered by Chebyshev Type I filters, and the passband edge frequency $f_p = 60$ Hz. The sampling frequency $f_s = 512$ Hz. All responses of the structure are recorded.

The modal parameters f_r, ζ_r, and ϕ_r are identified by the SSI method. Owing to the band-limited white noise, only the first seven modes can be obtained. According to (11) and (27), the 29 mass distribution vectors or the mass distribution matrices of the structure can be calculated by the unscaled mode shapes $[\Phi]$. In practice, according to (24), $N_0 = 5$. Therefore, at least five mode shapes of the structure are required to calculate the mass distribution vector or mass distribution matrix. A different total number of identified mode shapes can be used to calculate the mass distribution vectors, the details of which are shown in Table 1.

The mass distribution vectors calculated by the first seven modes are illustrated in Figure 2. Apparently, the given mass distribution vector is

$$\left\{\widetilde{M}_{\text{given}}\right\} = \left\{0.1564 \;\; 0.5349 \;\; 0.1893 \;\; 0.1564 \;\; 0.0247 \;\; 0.0741 \;\; 0.0247 \;\; 0.7741 \;\; 0.1317 \;\; 0.0823\right\}^T. \tag{31}$$

In Figure 2, the dark, thin solid lines coincide well with the thick dashed lines. Calculating the average of the 29 results, the identified mass distribution vector is

$$\left\{\widetilde{M}\right\} = \left\{0.1558 \;\; 0.5339 \;\; 0.1885 \;\; 0.1560 \;\; 0.0256 \;\; 0.0752 \;\; 0.0248 \;\; 0.7744 \;\; 0.1317 \;\; 0.0825\right\}^T. \tag{32}$$

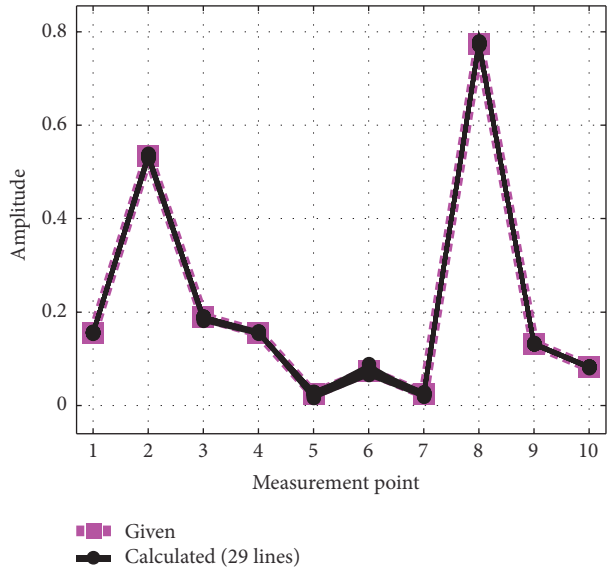

FIGURE 2: Mass distribution vectors calculated by the first seven modes.

The consistency of the lines means that the method used to calculate the mass distribution matrix is reliable.

3.2. Mass Matrix and Mass-Scaled Mode Shapes. To identify the mass matrix of the structure, a small mass, $\Delta m_9 = 1.0\,\text{kg}$, is added to DOF 9 of the structure. According to a method similar to that used in Section 3.1, $\{\widetilde{M}^{\delta}\}$ can be obtained as

$$\left\{\widetilde{M}^{\delta}\right\} = \{0.1550 \quad 0.5320 \quad 0.1886 \quad 0.1553 \quad 0.0241 \quad 0.0734 \quad 0.0244 \quad 0.7686 \quad 0.1715 \quad 0.0822\}^{T}. \tag{33}$$

According to (17) and (18), $\{m\}$ and $[M]$ can be acquired. The relative error between the given mass matrix $[M_{\text{given}}]$ and the identified mass matrix $[M]$ is shown in Table 2.

As can be seen from Table 2, the maximum relative error of the identified mass is 4.69% (DOF 5). Therefore, the relative error between the given mass matrix $[M_{\text{given}}]$ and the identified mass matrix $[M]$ is acceptable.

Since the mass matrix was obtained in Section 3.2, the mode scaling factor can be computed according to (20) and is given by

$$[\alpha] = \text{diag}\left(\{12.624 \quad 14.154 \quad 9.151 \quad 9.821 \quad 10.110 \quad 9.550 \quad 7.479 \quad 6.609 \quad 3.967 \quad 3.963\}^{T}\right). \tag{34}$$

According to (21) or (3), the mass-scaled mode shapes can be obtained.

4. Experimental Verification

To verify the aforementioned theory, a five-storey prototype structure was constructed for experimentation and is shown in Figure 3.

As can be seen from Figure 3, in this experiment, $f(t)$ is white noise. The acceleration responses $\{\ddot{x}(t)\} = \{\ddot{x}_1(t) \quad \ddot{x}_2(t) \quad \ddot{x}_3(t) \quad \ddot{x}_4(t) \quad \ddot{x}_5(t)\}^{T}$ are measured and stored by the SO Analyze© system (m+p international, Germany). The sampling frequency $f_s = 512\,\text{Hz}$.

The mode parameters are identified by the SSI method, and the stability diagram is reproduced in Figure 4. The natural frequency f_r and the damping ratio ζ_r are shown in Table 3.

Five modes can be identified. However, in Figure 4, the poles at the first modes are not as stable as the others. Meanwhile, the coherence functions at the first modes are not as satisfied as at the other modes. One reason for this is the fact that the responses of the first mode are larger than that of the others. This is also because the shaker in our laboratory is not good enough in the low frequency band. According to (24), $N_0 = 4$. Therefore, at least four modes shapes of the structure are required to calculate the mass distribution

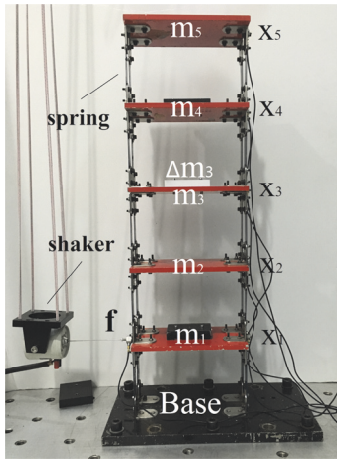

Figure 3: Experimental structure.

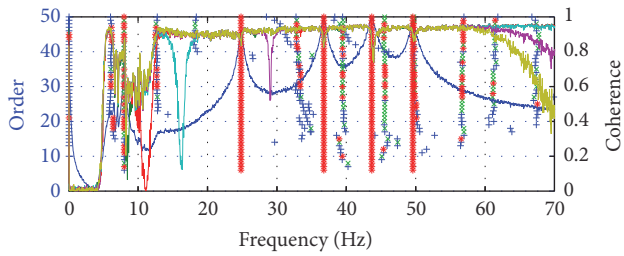

Figure 4: Stability diagram (∗, frequency and damping stability poles; ×, frequency stability poles; +, new poles).

Table 1: Total number of mass distribution vectors calculated by (27).

T	5	6	7
S_T	1	7	29

vector or mass distribution matrix. According to the stability diagram in Figure 4, the second, third, fourth, and fifth mode shapes are employed to calculate the mass distribution vector that is shown in Figure 5(a).

In Figure 5(a), the mass distribution vector can be identified as

$$\left\{\widetilde{M}\right\} = \{0.6100 \quad 0.3783 \quad 0.3711 \quad 0.5099 \quad 0.2951\}^T. \quad (35)$$

To identify the mass matrix of the structure, a small mass, $\Delta m_3 = 0.311$ kg, is added to DOF 3 of the structure. Repeated modal testing after changing the mass is undertaken. Similarly, the mass distribution vector of the modified structure can be computed, with the results shown in Figure 5(b). Then, $\{\widetilde{M}^\delta\}$ can be obtained as

$$\left\{\widetilde{M}^\delta\right\} = \{0.5961 \quad 0.3690 \quad 0.4250 \quad 0.4954 \quad 0.2874\}^T. \quad (36)$$

According to (17) and (18), $\{m\}$ and $[M]$ can be acquired, where

$$[M] = \mathrm{diag}(\{m\}) = \mathrm{diag}\left(\{2.9231 \quad 1.8130 \quad 1.7781 \quad 2.4453 \quad 1.4143\}^T\right). \quad (37)$$

According to (21) or (3), mass-scaled mode shapes can be obtained, which are shown in Figure 6. For comparison, the mass-scaled mode shapes estimated by EMA serve as the control group.

In Figure 6, the mass-scaled mode shapes obtained using EMA are represented by the light, thick, and dashed lines, while those identified using the proposed method are represented by the dark, thin, and solid lines. The dark, thin, and solid lines coincide with the light, thick, and dashed lines. The consistency of the dashed and solid lines means that the relative error between the mass-scaled mode shapes identified using EMA and those identified using the method proposed in this paper is acceptable.

5. Conclusions

In this paper, a mass-change-based method for the rescaling of mode shapes in OMA is introduced, which only requires response data. The features of the proposed method are listed as follows.

(1) The mass distribution matrix, which is defined as a diagonal matrix whose diagonal elements represent the ratios among the diagonal elements of the mass matrix, was calculated using the unscaled mode shapes given that the structure is discrete and the mass matrix is diagonal. Based on the theory of null space, the mass distribution vector or matrix was obtained.

(2) A small mass with calibrated weight was added to a certain DOF of the structure, and then the mass distribution vector of the modified structure was estimated. Based on the difference of the mass distribution vectors between the original and modified structures, the mass matrix was identified. In this method, the mass with calibrated weight was not necessary to be of light weight in order to minimize the difference between the original and modified structures.

(3) A universal set of modes was unnecessary when calculating the mass distribution matrix, indicating that modal truncation is allowed in the proposed method.

(4) A simulation was employed to validate the feasibility of the method. Furthermore, the method was tested on the output-only data from a five-storey structure under laboratory conditions. The mass-scaled mode shapes estimated by OMA according to the method proposed in this paper were compared with those obtained using EMA. The effectiveness of the method was confirmed and validated.

This method is not only enforceable in the simulation and experimental cases proposed in this paper but is also applicable for other engineering problems.

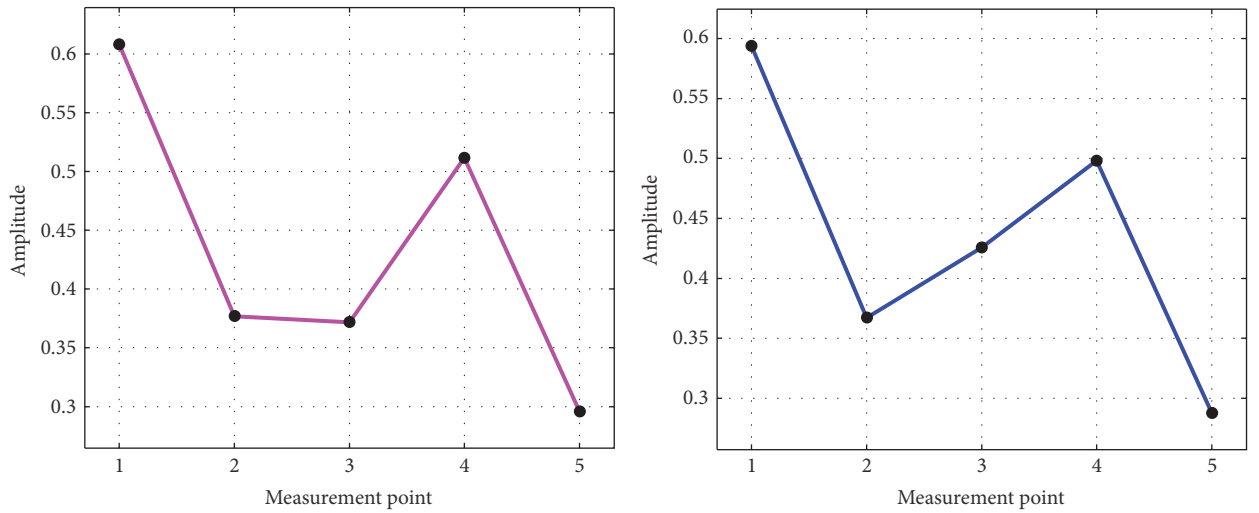

(a) Original structure (b) Modified structure

Figure 5: Mass distribution vector calculated by four modes.

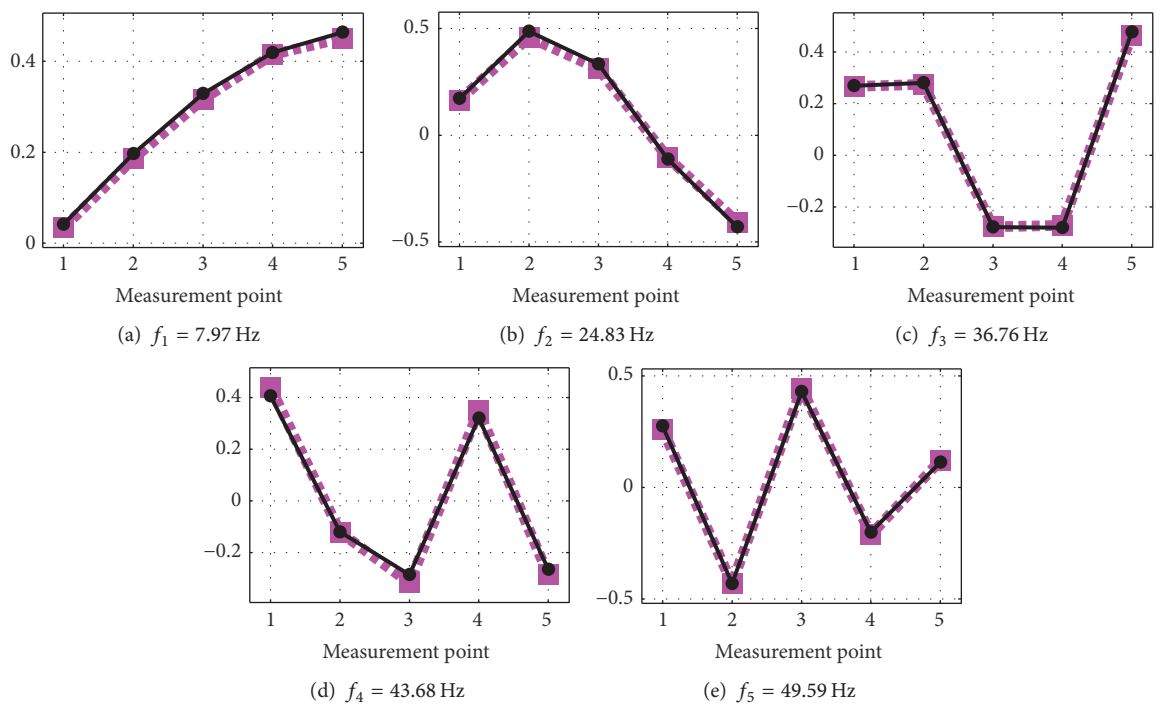

(a) $f_1 = 7.97$ Hz (b) $f_2 = 24.83$ Hz (c) $f_3 = 36.76$ Hz

(d) $f_4 = 43.68$ Hz (e) $f_5 = 49.59$ Hz

Figure 6: Mass-scaled mode shapes obtained using EMA (light, thick, and dashed lines) and the proposed method (dark, thin, and solid lines).

Table 2: Relative error between the given mass matrix $[M_{\text{given}}]$ and the identified mass matrix $[M]$.

DOF	1	2	3	4	5	6	7	8	9	10
$[M_{\text{given}}]$ (kg)	3.8	13.0	4.6	3.8	0.6	1.8	0.6	18.8	3.2	2.0
$[M]$ (kg)	3.820	13.094	4.622	3.826	0.628	1.843	0.609	18.991	3.231	2.022
Error (%)	0.52	0.73	0.48	0.69	4.69	2.41	1.56	1.02	0.96	1.10

Table 3: Identified mode frequencies and damping ratios.

Order	1	2	3	4	5
Frequency (Hz)	7.965	24.833	36.758	43.678	49.593
Damping ratio (%)	0.66	0.83	0.79	1.03	0.85

Conflicts of Interest

The authors declare that there are no conflicts of interest regarding the publication of this paper.

Acknowledgments

This research was supported by the National Natural Science Foundation of China under Grant no. 11272235.

References

[1] R. Brincker, "Some elements of operational modal analysis," *Shock and Vibration*, vol. 2014, Article ID 325839, 11 pages, 2014.

[2] B. L. Clarkson and C. A. Mercer, "Use of cross correlation in studying the response of lightly damped structures to random forces," *AIAA Journal*, vol. 3, no. 12, pp. 2287–2291, 1965.

[3] H. Akaike, "Power spectrum estimation through autoregressive model fitting," *Annals of the Institute of Statistical Mathematics*, vol. 21, pp. 407–419, 1969.

[4] S. R. Ibrahim, "Random decrement technique for modal identification of structures," *Journal of Spacecraft and Rockets*, vol. 14, no. 11, pp. 696–700, 1977.

[5] O. Døssing and C. H. Staker, "Operational deflection shapes: background measurement and application," in *Proceedings of the 5th International Modal Analysis Conference*, pp. 1372–1378, London, UK, 1987.

[6] G. H. James III, T. G. Carne, and J. P. Lauffer, "The natural excitation technique (NExT) for modal parameter extraction from operating structures," *Modal Analysis—The International Journal of Analytical and Experimental Modal Analysis*, vol. 4, pp. 260–277, 1995.

[7] B. Peeters, G. De Roeck, and T. Pollet, "Stochastic subspace techniques applied to parameter identification of civil engineering structures," in *Proceedings of the "New Advances in Modal Synthesis of Large Structures: Nonlinear Damped and Nondeterministic Cases"*, pp. 151–162, Lyon, France, 1995.

[8] S. W. Doebling and C. R. Farrar, "Computation of structural flexibility for bridge health monitoring using ambient modal data," in *Proceedings of the 11th Conference on Engineering Mechanics*, pp. 1114–1117, Fort Lauderdale, Fla, USA, May 1996.

[9] R. J. Guyan, "Reduction of stiffness and mass matrices," *AIAA Journal*, vol. 3, no. 2, p. 380, 1965.

[10] C. E. Ventura, J. F. Lord, M. Turek, R. Brincker, P. Andersen, and E. Dascotte, "FEM updating of tall buildings using ambient vibration data," in *Proceedings of the 6th International Conference on Structural Dynamics (EURODYN '05)*, pp. 237–242, Paris, France, 2005.

[11] H. Shahverdi, C. Mares, and J. E. Mottershead, "Model structure correction and updating of aeroengine casings using fictitious mass modifications," *Proceedings of the Institution of Mechanical Engineers, Part C: Journal of Mechanical Engineering Science*, vol. 219, no. 1, pp. 19–30, 2005.

[12] B. Schwarz and M. Richardson, "Using FEA modes to scale experimental mode shapes," in *Proceedings of the 24th Conference and Exposition on Structural Dynamics*, Saint Louis, Mo, USA, February 2006.

[13] B. Jaishi, H.-J. Kim, M. K. Kim, W.-X. Ren, and S.-H. Lee, "Finite element model updating of concrete-filled steel tubular arch bridge under operational condition using modal flexibility," *Mechanical Systems and Signal Processing*, vol. 21, no. 6, pp. 2406–2426, 2007.

[14] D. Hanson, R. B. Randall, J. Antoni, T. P. Waters, D. J. Thompson, and R. A. J. Ford, "Cyclostationarity and the cepstrum for operational modal analysis of MIMO systems—part II: obtaining scaled mode shapes through finite element model updating," *Mechanical Systems and Signal Processing*, vol. 21, no. 6, pp. 2459–2473, 2007.

[15] M. L. Aenlle and R. Brincker, "Modal scaling in operational modal analysis using a finite element model," *International Journal of Mechanical Sciences*, vol. 76, pp. 86–101, 2013.

[16] R. B. Randall, Y. Gao, and J. Swevers, "Updating modal models from response measurements," in *Proceedings of the 23rd International Conference on Noise and Vibration Engineering*, pp. 1153–1160, Leuven, Belgium, 1999.

[17] E. Parloo, P. Verboven, P. Guillaume, and M. Van Overmeire, "Sensitivity-based operational mode shape normalisation," *Mechanical Systems and Signal Processing*, vol. 16, no. 5, pp. 757–767, 2002.

[18] E. Parloo, P. Verboven, P. Guillaume, and M. Van Overmeire, "Force identification by means of in-operation modal models," *Journal of Sound and Vibration*, vol. 262, no. 1, pp. 161–173, 2003.

[19] R. Brincker and P. Andersen, "A way of getting scaled mode shapes in output only modal testing," in *Proceedings of the 21th International Modal Analysis Conference*, Orlando, Fla, USA, 2003.

[20] R. Brincker, J. Rodrigues, P. Andersen, and S. V. S. Aps, "Scaling the mode shapes of a building model by mass changes," in *Proceedings of the 22th International Modal Analysis Conference*, Dearborn, Mich, USA, 2004.

[21] D. Bernal, "Modal scaling from known mass perturbations," *Journal of Engineering Mechanics*, vol. 130, no. 9, pp. 1083–1088, 2004.

[22] D. Bernal, "A receptance based formulation for modal scaling using mass perturbations," *Mechanical Systems and Signal Processing*, vol. 25, no. 2, pp. 621–629, 2011.

[23] M. López-Aenlle, R. Brincker, F. Pelayo, and A. F. Canteli, "On exact and approximated formulations for scaling-mode shapes in operational modal analysis by mass and stiffness change," *Journal of Sound and Vibration*, vol. 331, no. 3, pp. 622–637, 2012.

[24] M. M. Khatibi, M. R. Ashory, and A. Malekjafarian, "Scaling of mode shapes using mass-stiffness change method," in *Proceedings of the 3rd International Operational Modal Analysis Conference*, pp. 699–706, Portonovo, Italy, 2009.

[25] M. López-Aenlle, P. Fernández, R. Brincker, and A. Fernández-Canteli, "Erratum to 'Scaling-factor estimation using an optimized mass-change strategy' [Mech. Syst. Signal Process. 24 (5)(2010) 1260–1273]," *Mechanical Systems and Signal Processing*, vol. 24, pp. 3061–3074, 2010.

[26] M. L. Aenlle, R. Brincker, A. F. Canteli, and L. M. Villa García, "Scaling factor estimation by the mass change method," in *Proceedings of the 1st International Operational Modal Analysis Conference (IOMAC '05)*, pp. 53–64, Copenhagen, Danmark, April 2005.

[27] P. Fernández, P. Reynolds, and M. López Aenlle, "Experimental evaluation of mass change approaches for scaling factors estimation," in *Proceedings of the 28th IMAC, A Conference on Structural Dynamics*, pp. 109–118, Springer, February 2010.

[28] P. Poozesh, D. D. Sabino, J. Baqersad, P. Avitabile, and C. Niezrecki, *Practical Techniques for Scaling of Optically Measured Operating Deflection Shapes*, Springer, Berlin, Germany, 2016.

[29] D. Bernal and B. Gunes, "Damage localization in output-only systems: a flexibility based approach," in *Proceedings of the 20th International Modal Analysis Conference (IMAC '02)*, pp. 1185–1191, Los Angeles, Calif, USA, February 2002.

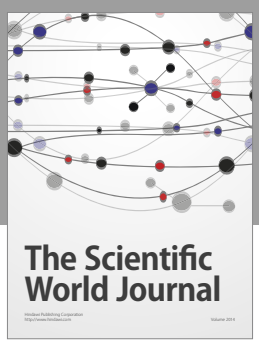

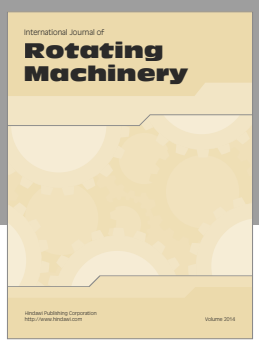

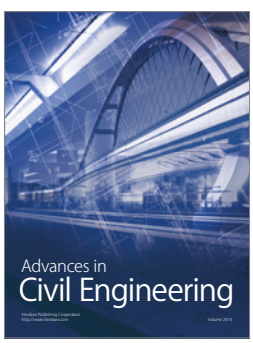

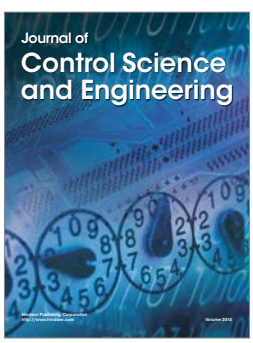

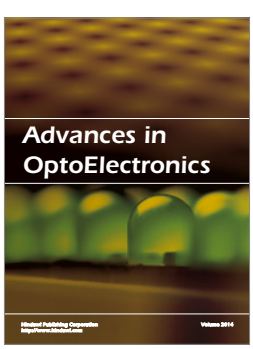

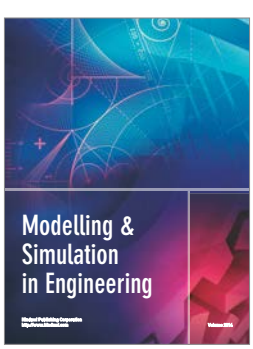

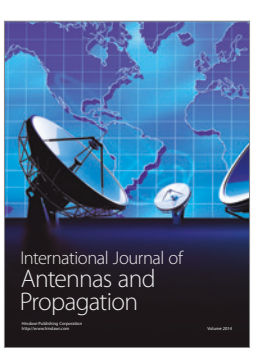

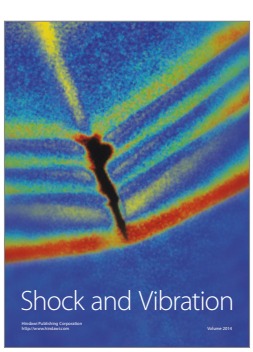

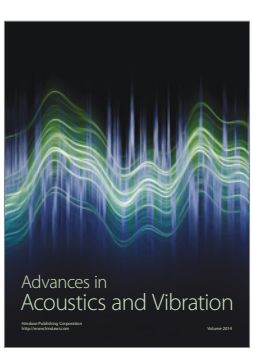

Hindawi

Submit your manuscripts at
https://www.hindawi.com